Bulletin of the Seismological Society of America, Vol. 72, No. 6, pp. 1843-1865, December 1982

ANALYSIS OF THE GROUND ACCELERATIONS RADIATED BY THE 1980 LIVERMORE VALLEY EARTHQUAKES FOR DIRECTIVITY AND DYNAMIC SOURCE CHARACTERISTICS

BY JOHN BOATWRIGHT AND DAVID M. BOORE

ABSTRACT

The strong motion accelerograph recordings of the 24 January 1980 main shock and the 27 January 1980 aftershock of the Livermore Valley earthquake sequence are analyzed for systematic variations with azimuth or station location. The variation of the peak accelerations with epicentral azimuth is apparently reversed for the two events: the main shock accelerations are larger to the south, and the aftershock accelerations are larger to the northwest. We eliminate the site effects by forming the ratio of the peak accelerations recorded at the same station, after correcting for the epicentral distance. This analysis indicates that source directivity caused a total variation of a factor of 10 in the peak accelerations. Comparison of this variation with the spatial extent of the aftershock sequences suggests that the strong directivity in the radiated accelerations is the result of unilateral ruptures in both events.

The accelerograms recorded at 10 stations within 35 km of the events were digitized to analyze the azimuthal variation of the rms acceleration, the peak velocity, and the radiated energy flux. The variation of rms acceleration correlates almost exactly with the variation of the peak accelerations. This correlation is analyzed using both deterministic and stochastic models for the acceleration waveforms. The peak velocities, corrected for epicentral distance, vary with azimuth by a factor of 5 for both events, while the radiated energy flux varies by a factor of 30 for the main shock and 15 for the aftershock. The peak velocities are strongly correlated with the radiated energy flux. The radiated seismic energies are estimated to be $2.6 \pm 0.9 \times 10^{20}$ dyne-cm for the main shock and $1.5 \pm 0.3 \times 10^{20}$ dyne-cm for the aftershock.

INTRODUCTION

The azimuthal variation of the radiated seismic energy due to the geometry of the rupture growth, or directivity, has long been recognized at intermediate periods (several tens of seconds) in teleseismic recordings of large earthquakes (e.g., Benioff, 1955). The existence of strong directivity effects at shorter periods, especially at periods of engineering interest, is a matter of current debate. Recordings of ground accelerations from several recent earthquakes in California including the 1971 San Fernando (McGuire and Hanks, 1980), 1979 Coyote Lake (Archuleta, 1979), and Imperial Valley (Swanger *et al.*, 1981) have been interpreted as showing directivity.

Although convincing, the evidence is not indisputable. Objections that have been raised to this interpretation appeal to considerations of the heterogeneity of the stress release in an extended rupture and systematic effects due to radiation pattern, local soil amplification, foundation-soil interaction, and anelastic attenuation. While these competing effects cannot possibly obviate all these interpretations, they hinder the direct quantification of directivity.

In this paper, we present what appears to be unambiguous evidence for directivity in the accelerations radiated by two earthquakes which occurred near Livermore Valley, California, during January 1980. The analysis for directivity is enhanced by the good azimuthal coverage, the moderate size of the faults relative to the distance

from the stations, and the fact that many stations recorded both events. By comparing the accelerations recorded at the same stations, it is possible to eliminate many of the difficulties associated with analyzing data from a single event. The peak acceleration data were first presented as part of a letter to the editor by Boore and Porcella (1980); this paper presents a more complete analysis of the accelerograms written by these earthquakes.

While peak acceleration is the most prevalent quantification of strong ground motion, there are other measurements which may be analyzed to test the directivity in the radiated wave field; in particular, we have analyzed the rms acceleration, the peak velocity, and the radiated energy flux of the *S*-wave arrivals at 10 of the closest stations. The peak velocity and the radiated energy flux (the integral of the square of the ground velocity) are velocity analogs of the peak and rms acceleration; the energy flux, uncorrected for attenuation, is proportional to the square of the rms velocity times the signal duration. This work presents the first observational analysis of directivity in these integral measures of strong ground motion.

The Livermore Valley Earthquakes

The Livermore Valley earthquakes provide an excellent opportunity to study directivity in high-frequency ground motion. Both the main shock and the largest aftershock were well recorded by strong motion accelerographs (Figure 1). The main shock occurred on 24 January 1981 at a hypocentral depth of 10.5 km and had a moment of about 6×10^{24} dyne-cm. The moment of the largest aftershock, which occurred on 27 January 1981, at a depth of 15 km, was about 2×10^{24} dyne-cm (Bolt *et al.*, 1981; J. F. Scheimer, oral communication, 1982). Short-period *P*-wave first motions indicate that the faulting involved strike-slip motion on near-vertical planes. The main shock had a short-period *P*-wave nodal plane striking 11° west of north, while the aftershock had a nodal plane striking 37° west of north (Cockerham *et al.*, 1980). Figure 2 shows the epicentral locations of the aftershocks which occurred within 24 hr of the main shock. The aftershock sequence indicates that the main shock rupture propagation was primarily to the southeast. The trend of the aftershock sequence is rotated 25° from the strike of the north-south nodal plane of the main shock focal mechanism, but is parallel to the strike of the aftershock nodal plane. As discussed in the next section, the peak motions radiated by the main shock arrive relatively late in the waveforms. In the analysis for the directivity, these motions are assumed to be radiated by the section of the fault which strikes to the southeast; the short-period focal mechanism is assumed to correspond only to a small initial rupture event.

Figure 3 shows the seismicity pattern for a 5-hr period on either side of the 27 January aftershock; 2- and 24-hr periods show similar patterns. The rupture in the aftershock appears to have propagated to the northwest; this direction is inferred from the cluster of small earthquakes to the northwest of the epicenter. As Figure 2 shows, however, the region of supposed aftershocks of the 27 January event is also the site of aftershock activity following the main shock. These clusters may represent the response of an unruptured asperity between the two events and not indicate rupture propagation to the northwest in the 27 January aftershock.

The Strong Motion Accelerograms

A subset of the accelerograms written by the 24 January main shock are shown in Figure 4, superimposed on a map of the region showing the town of Livermore and the Sacramento River. The accelerations plotted to the right of the station locations are the *SH* components of the horizontal motion. The amplitudes of the

accelerations are scaled to correct for the geometrical spreading using the hypocentral distances listed in Table 2. The fault plane inferred from the aftershock distribution is drawn as a dark wavy line. The directivity in the radiated accelerations is clearly demonstrated by the difference in amplitude between station DVD to the south and stations ANT and WCS to the northwest. This variation with azimuth is reversed in Figure 5, which shows the accelerograms written at the same stations by the 27 January aftershock. The accelerations radiated by the aftershock are larger at ANT and WCS than at DVD while they are approximately the same for the stations to the east and west.

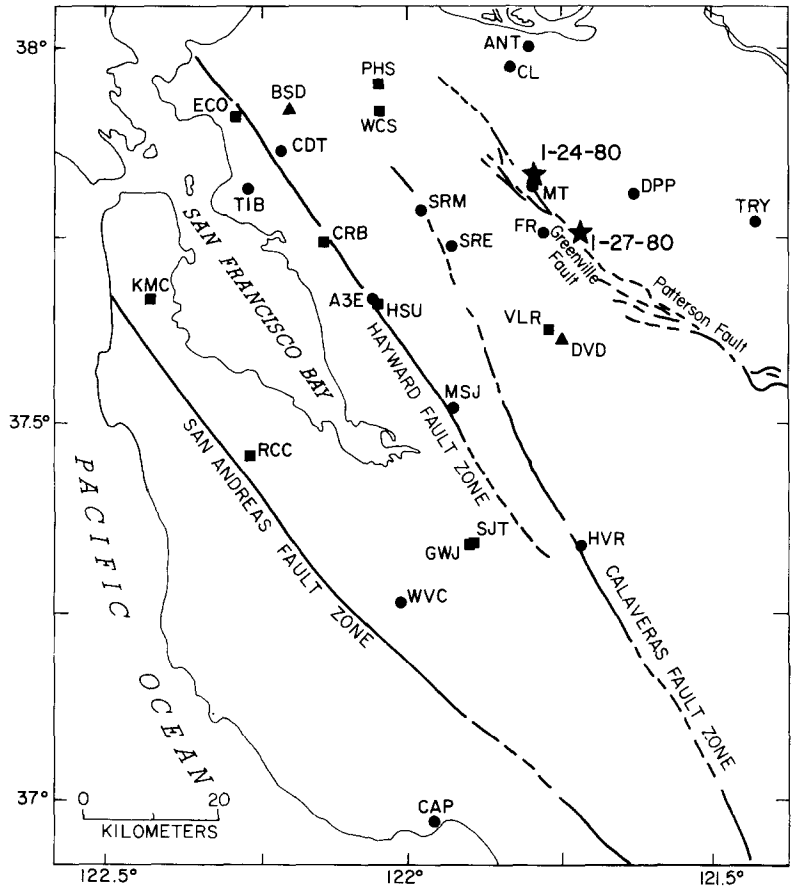

FIG. 1. Location map, adapted from McJunkin and Ragsdale (1980). Epicenters of the 24 and 27 January events (Cockerham *et al.*, 1980) are shown by stars. Permanent and temporary accelerograph stations shown by three- and two-letter designations, respectively (McJunkin and Ragsdale, 1980; Switzer *et al.*, 1981). Temporary stations were installed after the 24 January event. Structure type indicated by symbol: circle, building less than three stories; square, building taller than two stories; triangle, dam abutment or toe.

In addition to the strong difference in the azimuthal variation of the amplitudes radiated by the two earthquakes, there is a significant difference in the character of the acceleration waveforms. The peak accelerations in the main shock accelerograms arrive relatively late in the waveforms, whereas the peak accelerations in the aftershock accelerograms occur as the second pulse. This difference is assumed to reflect the complexity of the rupture process of the main shock relative to that of the aftershock. In the main shock, the initial motions of the accelerograms are

radiated by an initial rupture event whose focal mechanism is given by the short-period P-wave radiation pattern. The peak motions in the accelerograms are associated with rupture on the southeast extension of the aftershock distribution. The peak motions in the waveforms radiated by the 27 January event are interpreted

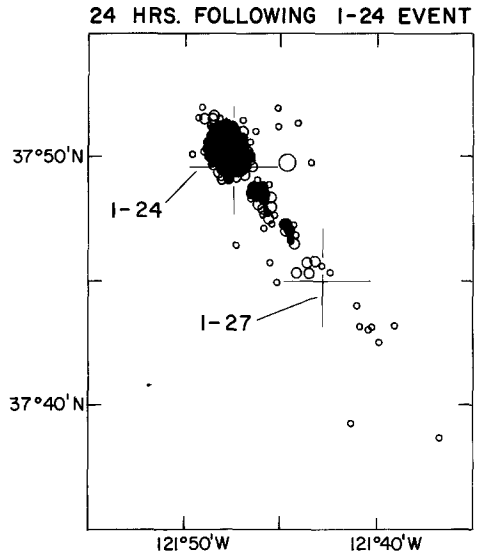

FIG. 2. Aftershocks for 24 hr following the 24 January event, with magnitude shown by symbol size (∘ for $M_L > 2.0$, ○ for $M_L > 4.0$). Locations of the 24 and 27 January events are indicated by crosses.

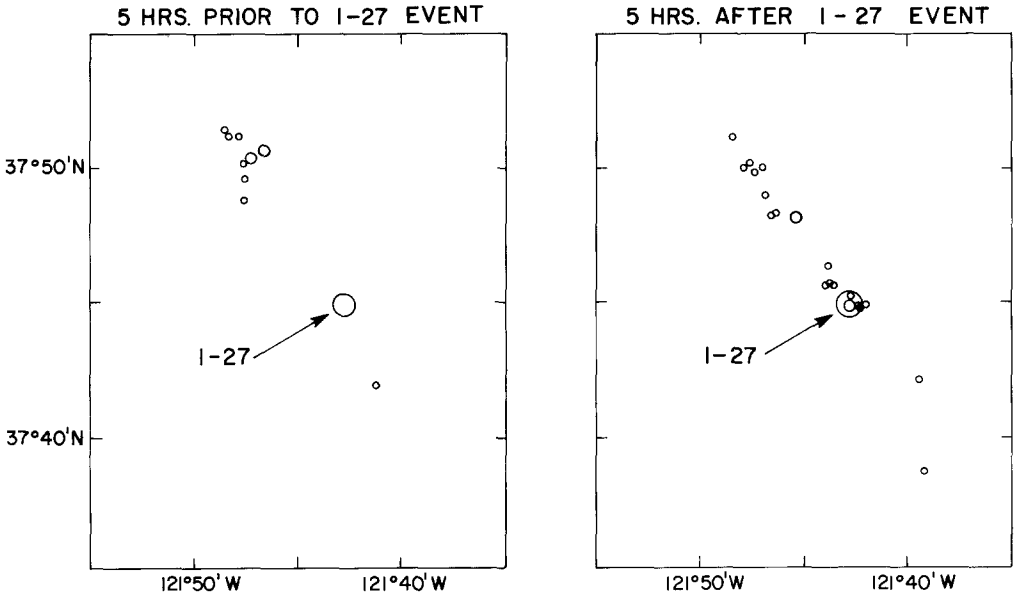

FIG. 3. Aftershocks for 5-hr periods before and after 27 January event (shown by largest symbol).

as examples of stopping phases, i.e., the acceleration pulses radiated by the deceleration of a rupture front (Savage, 1965; Madariaga, 1977), as their polarities are reversed with respect to the first motion of the waveforms.

Before analyzing these accelerations, it is useful to consider some of the site

effects in the data by comparing accelerograms from stations which are near the same azimuth from the epicenters of the events. In Figure 6, we have plotted the *SH* components of the acceleration recorded at stations DVD and VLR, which are separated by 1 km. Although the relative amplitudes are similar, the site response

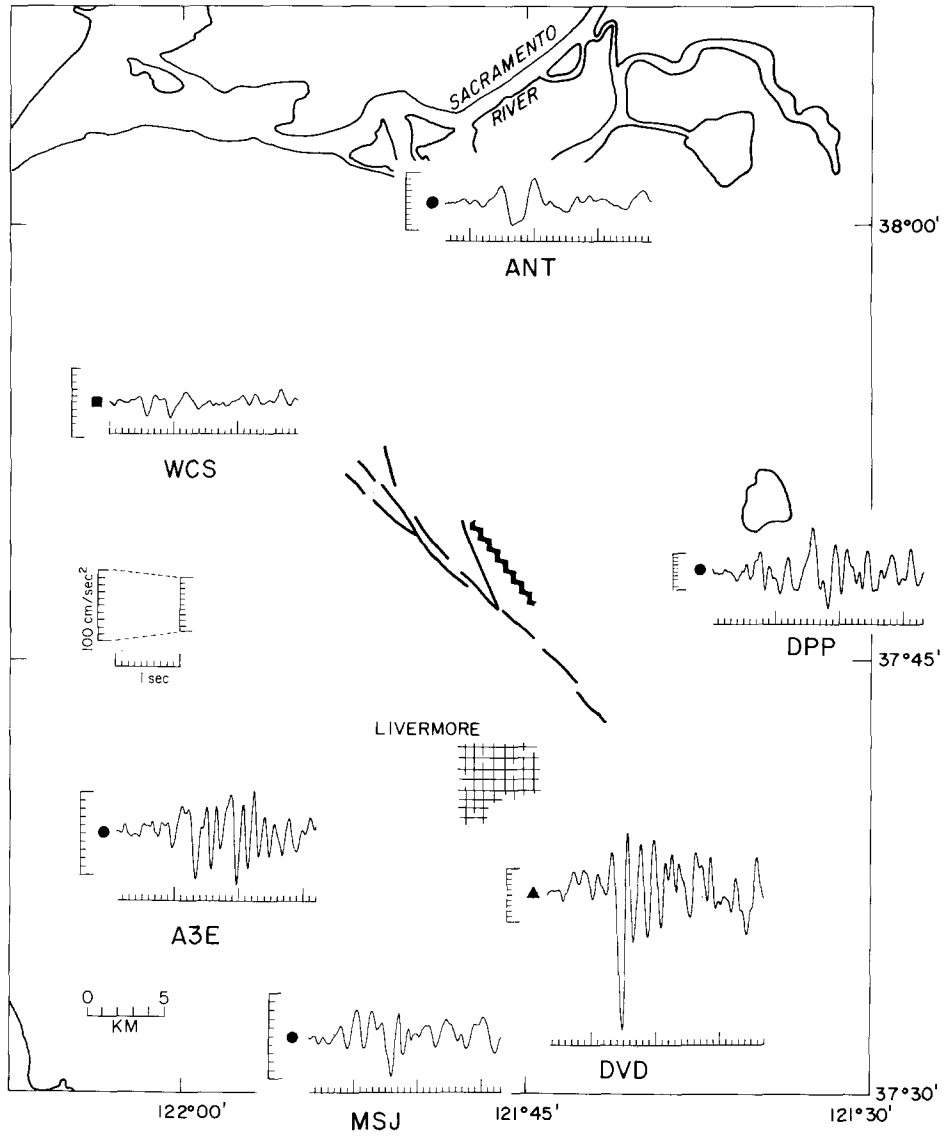

FIG. 4. Selected *SH* accelerograms of the 24 January main shock superimposed on a map of the Livermore area, showing the directivity in peak motions and relative complexity of the main shock accelerograms. The acceleration scales have been adjusted to compensate for the expected geometrical spreading; the scales are 100 cm/sec^2 between the large tick marks.

of the two stations differs strongly. The Del Valle Dam toe has a strong resonance at 8 Hz, and the Veterans Administration Hospital resonates at about 0.4 Hz (R. B. Matthiesen, oral communication, 1980). Because these resonant frequencies are somewhat outside the peak frequency of the ground acceleration at these stations,

the different responses have relatively little effect on the measurements of the peak and rms acceleration, other than to slightly amplify the motions at DVD for the 24 January main shock.

Figure 7 shows a more extreme example of differential site effects, using the accelerograms written at three stations whose azimuths from the epicenters are within 25° of each other. Stations SRE and SRM are less than 5 km from each

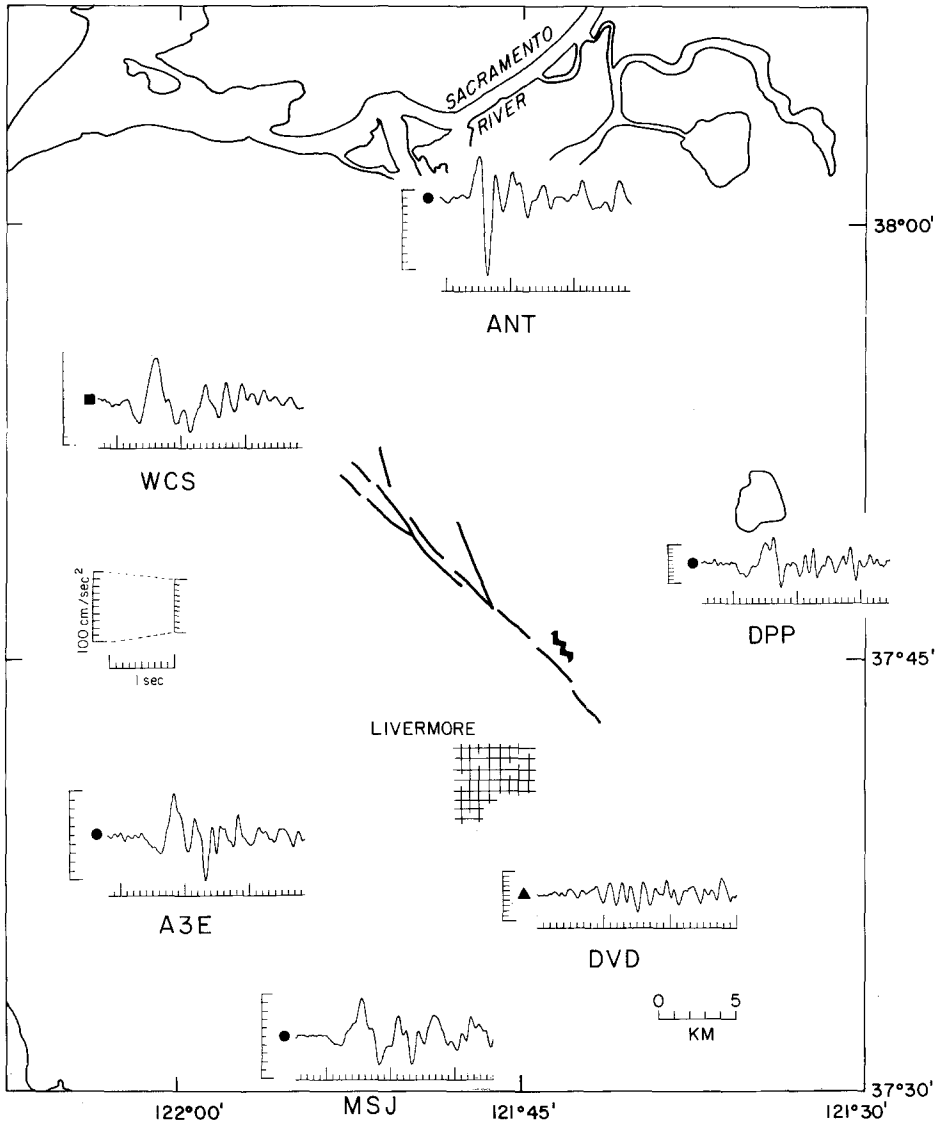

FIG. 5. Selected *SH* accelerograms of the 27 January aftershock. The acceleration scales have been adjusted as in Figure 4. Note the strong amplification to the northwest, relative to the 24 January accelerograms.

other, yet their accelerograms are remarkably different. The Eastman Kodak Building has a strong site amplification at 1.5 Hz, as the large acceleration pulses in both records indicate, while the San Ramon Fire Station appears to have a broad spectral hole around 1 Hz. Because the acceleration radiated by the main shock is strongest at these frequencies, the differences in the waveforms and in the peak and

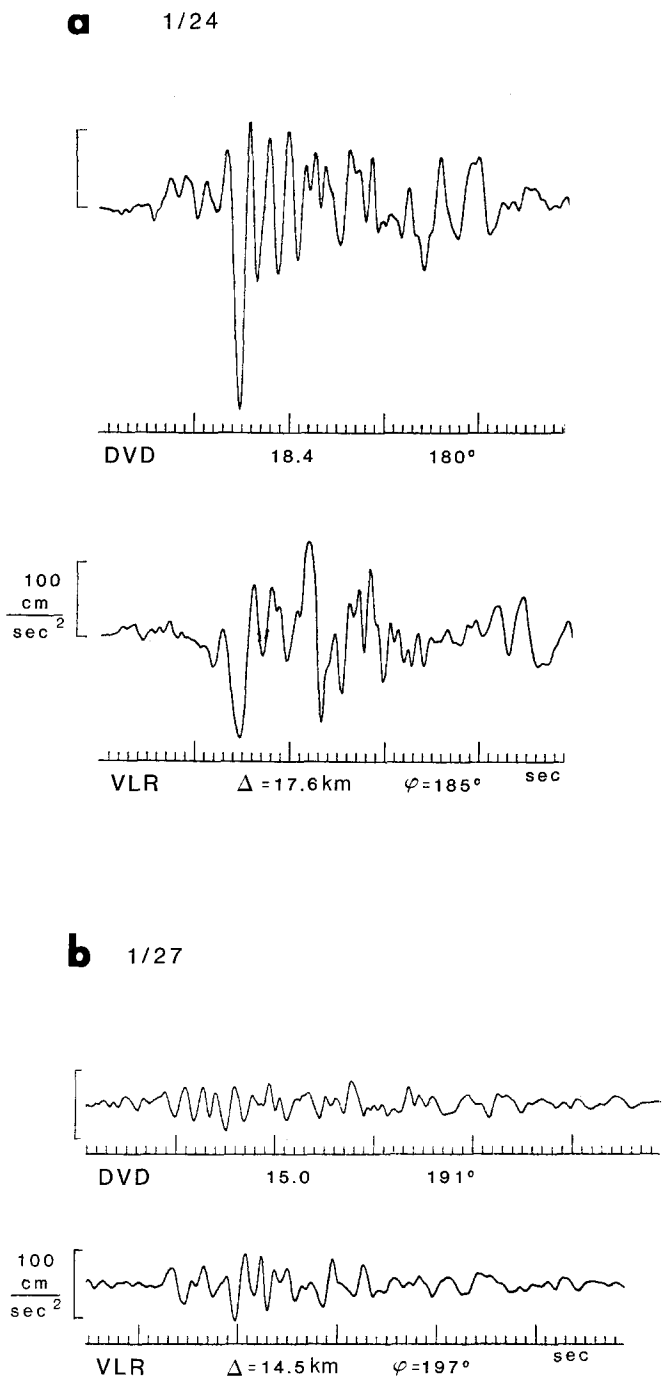

FIG. 6. (a) *SH* accelerograms of the 24 January main shock recorded at stations DVD and VLR. The scales are adjusted as in Figures 4 and 5. Distance and azimuth from the epicenter are indicated below the accelerograms. (b) *SH* accelerograms written by the 27 January aftershock at the same stations.

rms acceleration measurements are pronounced. The accelerograms recorded at station A3E are shown as a control for the comparison of SRE and SRM, although A3E has a site resonance at about 6 Hz. The accelerograms written by the aftershock at SRE and A3E are remarkably similar in shape. Because of the site amplification,

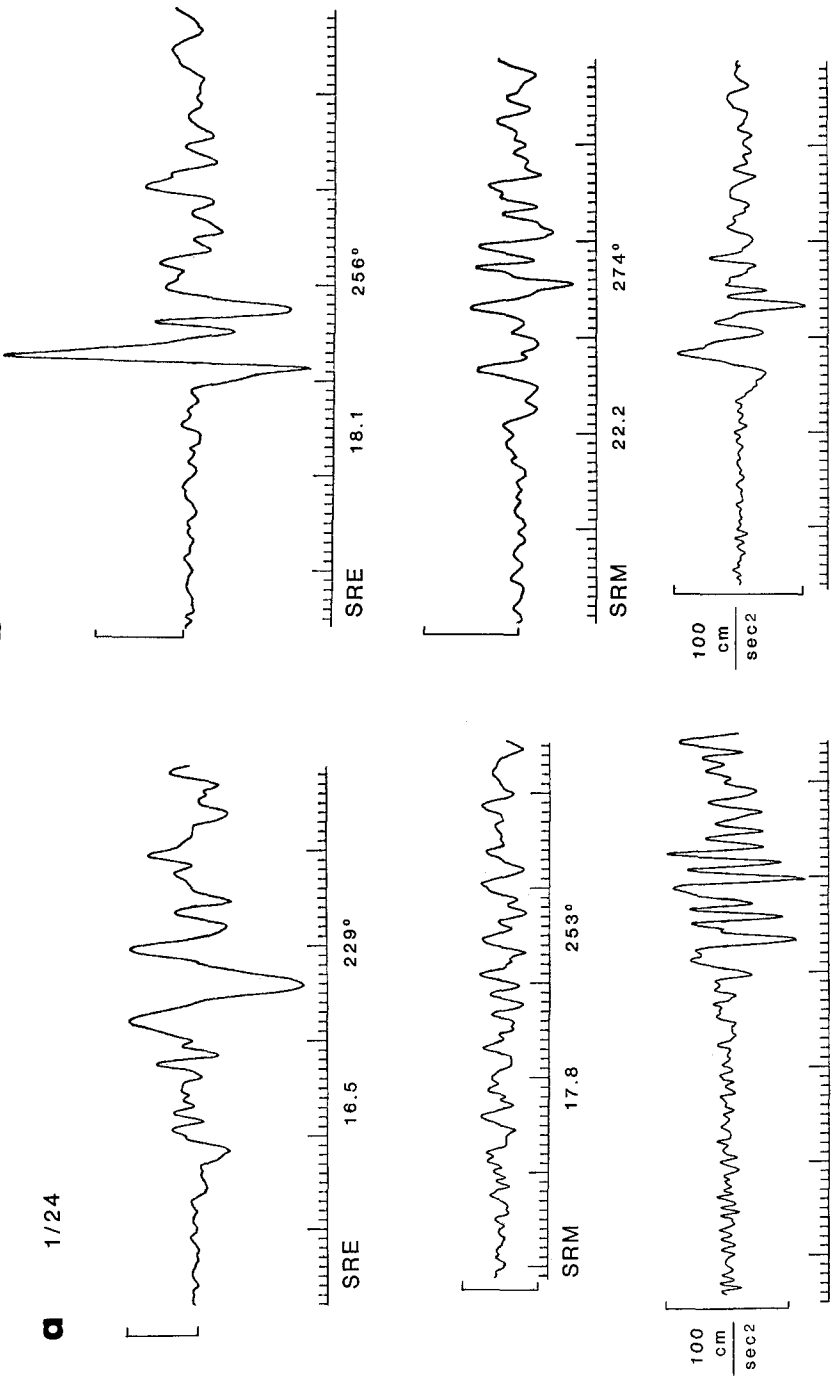

Fig. 7. (a) *SH* accelerograms of the 24 January main shock recorded at stations SRM, SRE, and A3E. (b) *SH* accelerograms written by the 27 January aftershock at the same stations.

however, the accelerograms recorded at SRE are not used to estimate source parameters.

Peak Ground Accelerations

Despite these pronounced site effects, because of the large number of stations which recorded both of the events, this data set is of considerable use for studying

TABLE 1

Peak Acceleration Data

Station	Structure Type*	24 January Event			27 January Event		
		d† (km)	ϕ	Peak Ground Acceleration‡ (g)	d (km)	ϕ	Peak Ground Acceleration (g)
A3E	1	30.6	232°	0.065	31.7	247°	0.065
ANT	1	21.0	354°	0.045	28.4	345°	0.112
BSD	3	38.4	284°	0.016	45.2	291°	0.044
CAP	1	92.0	191°	0.023		No Record	
CDT	1	38.4	277°	0.020		No Record	
CRB	2	33.4	253°	0.016	37.2	265°	0.026
DPP	1	11.3	80°	0.12	9.9	56°	0.071
DVD	3	18.4	180°	0.26	15.0	191°	0.047
ECO	2	45.9	280°	0.005	52.4	286°	0.010
GWJ	2	51.1	195°	0.011	48.4	199°	0.005
HSU	2	30.4	231°	0.048	31.4	247°	0.059
HVR	1	49.3	176°	0.093		No Record	
KMC	2	60.4	252°	0.017	63.7	259°	0.012
MSJ	1	32.0	209°	0.056	30.4	217°	0.039
PHS	2	27.6	300°	0.033	35.5	305°	0.035
RCC	2	59.7	226°	0.011	59.4	234°	0.003
SJT	2	51.0	194°	0.023	48.3	199°	0.006
SRE	1	16.5	229°	0.154	18.1	256°	0.275
SRM	1	17.8	253°	0.052	22.2	274°	0.058
TIB	1		No Record		47.9	276°	0.026
TRY	1	28.8	93°	0.086		No Record	
VLR	2	17.6	185°	0.17	14.5	197°	0.059
WCS	2	26.0	290°	0.032	33.4	298°	0.057
WVC	1	62.4	202°	0.018	60.2	206°	0.012
CL	1	Station Not Installed			24.1	339°	0.026
FR	1	Station Not Installed			4.1	246°	0.259
MT	1	Station Not Installed			8.1	314°	0.267

* Station identification, coordinates, and structure type (1 = buildings less than or equal to two stories, 2 = buildings larger than two stories, 3 = dam toe or abutment) from Switzer *et al.* (1981). CL, FR, and MT are temporary stations installed after the 24 January event (McJunkin and Ragsdale, 1980).

† Closest horizontal distance and azimuth from source to station, assuming faults extending from 37.827°N, 121.787°W to 37.783°N, 121.746°W and 37.750°N, 121.713°W to 37.768°N, 121.729°W for the 24 and 27 January events, respectively. Fault locations based on earthquake locations by Cockerham *et al.* (1980).

‡ Peak ground acceleration, largest of the two horizontal components scaled from original records by R. L. Porcella.

directivity. In this section, the peak ground accelerations are analyzed to estimate the directivity in each event. The peak motion (PGA) is defined as the largest acceleration of the two horizontal components; the values were scaled off the original records by R. L. Porcella (Table 1) and have uncertainties of about $\pm$ 0.005 g. In order to isolate azimuthal variation of peak motions for each event, the effects of

attention and geometrical spreading must be removed. We have divided the observed peak accelerations by the peak accelerations predicted from the attenuation curves of Joyner and Boore (1981).

$$\log PGA = -1.02 + 0.249M - \log r - 0.00255r$$
$$r = (d^2 + 7.3^2)^{1/2}, \quad (1)$$

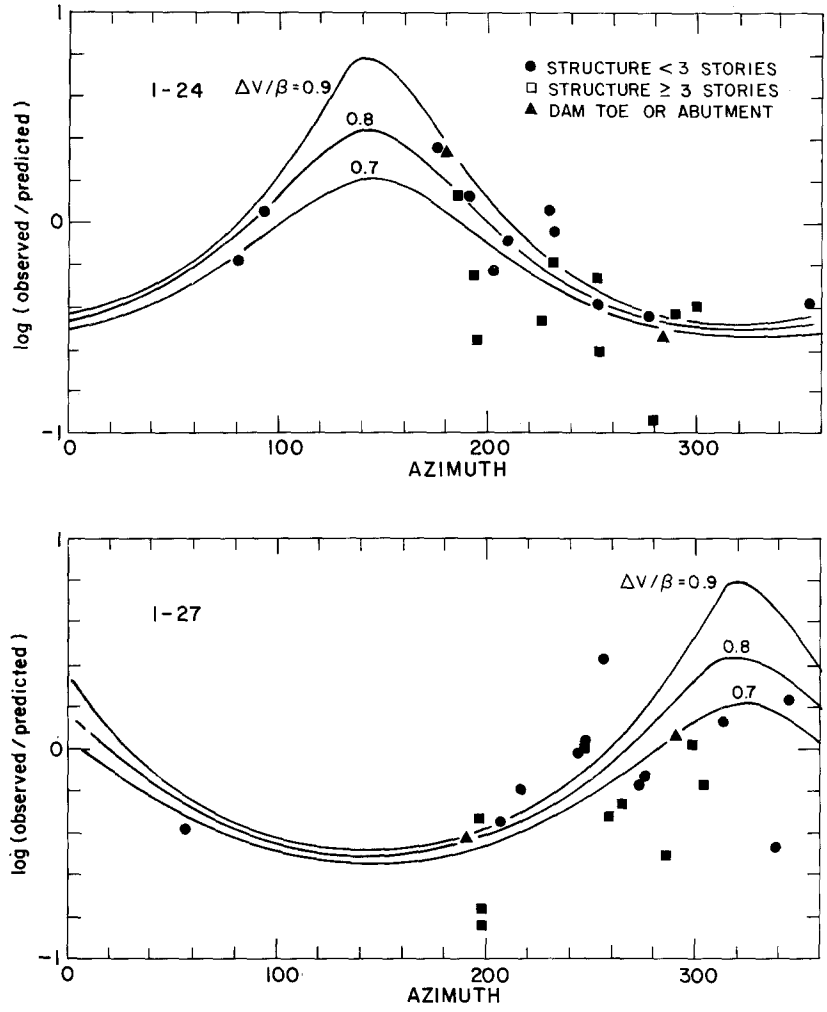

FIG. 8. The logarithms of the observed peak acceleration divided by the predicted peak acceleration, plotted against azimuth from source to receiver. The predicted motions are estimated from equation (1), using moment magnitudes of 5.8 and 5.5 for the 24 and 27 January events. The curves superimposed on the data are the theoretical predictions determined from equation (2) adjusted vertically to the data.

where M is moment magnitude of the earthquake and d is the closest distance to the surface projection of the fault rupture in kilometers. The corrected peak accelerations are plotted in Figure 8; they show markedly different variations with azimuth for the two events. The azimuthal variation for the peak accelerations recorded in the basements of large and small structures is approximately the same, but the two sets of data differ from one another by a constant factor. This is

consistent with analyses of the accelerations from other earthquakes, especially the 1971 San Fernando event. The peak accelerations recorded in the basements of tall buildings are less than those recorded in small structures: Boore *et al.* (1980) find the difference to be 0.2 log units for the San Fernando data. Considering this effect of structure size, the estimates of the total azimuthal variation of the peak accelerations yields a factor of 8 for the main shock (0.9 log units) and a factor of 5 for the aftershock (0.7 log units).

A critical consideration in this analysis is the effect of the radiation patterns. It is not possible to discern the *SH* nodes, predicted at 188° and 278°, in the measurements of peak acceleration shown in Figure 8. Although this difficulty does not rule out the possibility that the radiation patterns influence the peak accelerations, the dense sampling of station azimuths from 180° to 300° indicates that the radiation patterns are significantly obscured. The radiation patterns are assumed to be obscured by two effects: the scattering of body waves at high frequencies and the complexity of the dynamic rupture process. Note also that the peak horizontal *S*-wave motion is measured without regard to whether it is *SH* or *SV* motion.

As discussed earlier, it is difficult to estimate directivity for single events: apparent azimuthal variations can be caused by coarse sampling of radiation patterns, by using improper distance corrections, or by azimuthally dependent geology and structure-size distributions. To eliminate these effects, we have analyzed the ratio of peak accelerations at those stations which recorded both events. Because the epicentral distances are similar, this ratio is relatively insensitive to the attenuation relation used to correct for the epicentral distance. The results plotted in Figure 9 show a marked azimuthal dependence, with a total variation of a factor of 30 (1.5 log units). Because we are using the ratio of the peak accelerations at these stations, this variation can only result from the directivity in the two events. If the dominant motion of the main shock occurred on the same fault plane as the aftershock, as suggested by the aftershock sequence following the main shock, this ratio also eliminates any bias which might result from the radiation patterns.

It is important to analyze the azimuthal variations using theoretical predictions of directivity. As a simple model for the variation of the peak ground acceleration, we consider the directivity function,

$$D^s(\psi) = [1 - \frac{\Delta v}{\beta} \cos \psi]^{-1} \tag{2}$$

(Madariaga, 1977; Boatwright, 1982) where Δv is the change of rupture velocity associated with the radiation of the acceleration pulse, β is the shear wave velocity at the source, and ψ is the angle between the direction of rupture and the takeoff direction of the ray. This equation is exactly applicable only for the peak accelerations measured from the acceleration pulses radiated by the same faulting event. In calculating the theoretical curves, the takeoff angles of the rays are assumed to be horizontal; ψ is taken as the angle between the rupture direction, ϕ_r, and the azimuth to the station, ϕ. The rupture directions were assumed to be horizontal and aligned with the southeastward extension of the distribution of aftershocks for the main shock ($\phi_r = 143°$) and with the northwest ($\phi_r = 323°$) for the aftershock. The theoretical curves calculated for $\Delta v = 0.7\beta$, 0.8β, and 0.9β are plotted on Figures 8 and 9. The curves in Figure 8 were adjusted vertically to the small structure data.

Although it is not possible to choose between the changes of rupture velocity, the agreement of the theoretical curves with the main shock data is surprisingly good. Because of the increased scatter of the data, however, the fit of the theoretical curves to the aftershock data is less convincing.

In Figure 9, the theoretical curves are compared to the ratios of the peak accelerations: the agreement is remarkable in that no free parameters were varied to obtain it. Using only the small-structure and dam site data, the change of rupture velocity appears to be greater than 0.7β. The takeoff angles of the shear waves recorded at stations 10 to 35 km from the epicenters range from 40° to 10° above horizontal (R. Cockerham, written communication, 1981). For a purely horizontal rupture, this range of takeoff angles weakens the expected directivity by approximately 10 per cent. The directivity would also be weakened if the directions of the ruptures were not purely horizontal. These two considerations indicate that the theoretical curves calculated using $\psi = \phi - \phi_r$ represent upper bounds for the expected directivity. Therefore, $\Delta v = 0.7\beta$ is a strong lower bound for the change of rupture velocity.

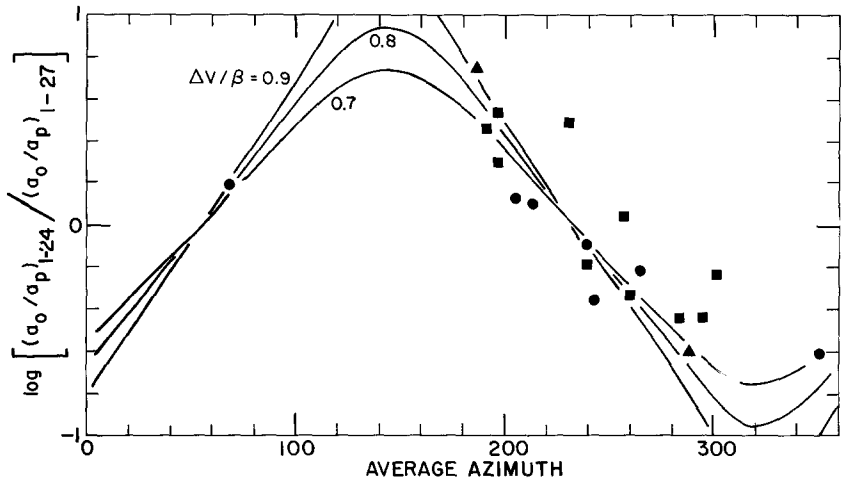

FIG. 9. The logarithms of the ratio of peak accelerations from the 24 and 27 January events corrected for distance with theoretical curves determined for various changes of rupture velocity superimposed.

In order to consider the variation of peak acceleration which may result from differential site effects or radiation patterns, we analyze the distribution of the logarithms of the products, at each station, of the corrected peak accelerations. Assuming that the directivity in the two events is exactly reversed in azimuth and equal in amplitude, the standard deviation of this distribution is equal to twice the variation which may be attributed to site effects. This procedure estimates the total peak to peak variation expected from site effects and radiation patterns as a factor of 3 (half a log unit).

RMS ACCELERATIONS

We have analyzed the rms accelerations of the *SH* components of the shear waves radiated by the main shock and the largest aftershock using a subset of the stations which recorded the two events. The stations chosen represent as complete an azimuthal distribution as possible; they also include most of the strong motion stations within 35 km of the two events.

While mostly *SH* motion, the shear waves are not perfectly polarized. Because the *SH* component is always the largest component of motion, however, this analysis is consistent with the previous analysis of the peak ground acceleration. The measurements of a_{rms} and the durations used to calculate them are shown in Table 2. The choice of the interval over which the square of the acceleration is averaged was made in a subjective fashion, where the direct *S* wave is enclosed as closely as possible. As discussed by McCann and Boore (1982), this technique, although subjective, is well conditioned; varying the duration has little effect on the rms estimates.

To isolate the variation of these measurements with azimuth, we multiply the rms acceleration by the hypocentral distance, to correct for the geometrical spreading. The resulting estimates are then averaged to obtain the mean $\overline{Ra_{rms}}$, and the logarithm of $Ra_{rms}/\overline{Ra_{rms}}$ is calculated. These logarithms are plotted in Figure 10, along with the logarithms of the observed peak accelerations divided by the predicted peak accelerations for the same stations. The corrected a_{rms} values track the corrected peak acceleration values well: the corrected values are more than 25 per cent from each other at only four of the stations.

TABLE 2

RMS ACCELERATION DATA

Station	24 January Event					27 January Event			
	R^* (km)	τ (sec)	a_{rms} (cm/sec^2)	f_{max} (Hz)	$\Delta\sigma$ (bars)	R (km)	τ (sec)	a_{rms} (cm/sec^2)	$\Delta\sigma$ (bars)
A3E	32.4	1.52	27.0	6.0	137	35.1	1.33	19.8	164
ANT	23.5	1.10	22.5	2.0	125	32.1	0.90	35.2	266
DPP	15.4	1.61	46.3	4.5	137	18.0	0.95	31.1	132
DVD	21.2	1.20	84.9	5.0	321	21.2	1.34	15.2	76
MSJ	33.7	1.43	17.6	4.0	125	33.9	1.53	17.8	142
SRE	19.6	1.87	56.6	2.0	286	23.5	1.04	89.3	494
SRM	20.7	2.09	16.5	4.0	72	26.8	1.70	28.1	177
VLR	20.5	1.47	60.8	4.5	240	20.9	1.30	17.4	86
WCS	28.0	1.53	8.7	2.0	57	36.6	1.14	21.9	189
FR	Station Not Installed					15.6	0.88	89.9	330

* Hypocentral distance computed from nearest epicentral distances listed in Table 1 and the hypocentral depths of 10.5 km for the main shock and 15 km for the aftershock.

The correlation is somewhat stronger than the correlation presented by Hanks and McGuire (1981) for the accelerograms written by the 1975 Oroville aftershock sequence. If we use this correlation to extrapolate the variation of the corrected peak accelerations to the corrected rms accelerations, we then estimate a directivity effect of a factor of 10 (peak to peak) for measurements of rms acceleration from a strongly unilateral event.

As demonstrated by Boatwright (1982), the rms acceleration may be used to estimate the rms dynamic stress drop averaged over the rupture area. In general, the relation between the rms acceleration and the rms dynamic stress drop depends on the shape of the acceleration spectrum. For acceleration spectra which are flat between the corner frequency, f_0, and a high-frequency limit, f_{max}, we can use the relation,

$$\Delta\sigma = 1.13 \frac{\rho}{\bar{\mathcal{R}}^s} \frac{\beta^2}{v\Delta v} \left(\frac{f_{max}}{f_0} - 2 \right)^{-1/2} \overline{Ra_{rms}} \tag{3a}$$

(Boatwright, 1982). This spectral model is appropriate for the accelerations radiated by the main shock. For acceleration spectra where $f_{max} < 5f_0$ or which fall off as ω^{-1} above the corner frequency, this relation may be rewritten as,

$$\Delta\sigma = \frac{2}{3}\frac{\rho}{\bar{\mathcal{R}}^s}\frac{\beta^2}{v\Delta v}\overline{Ra}_{rms}. \tag{3b}$$

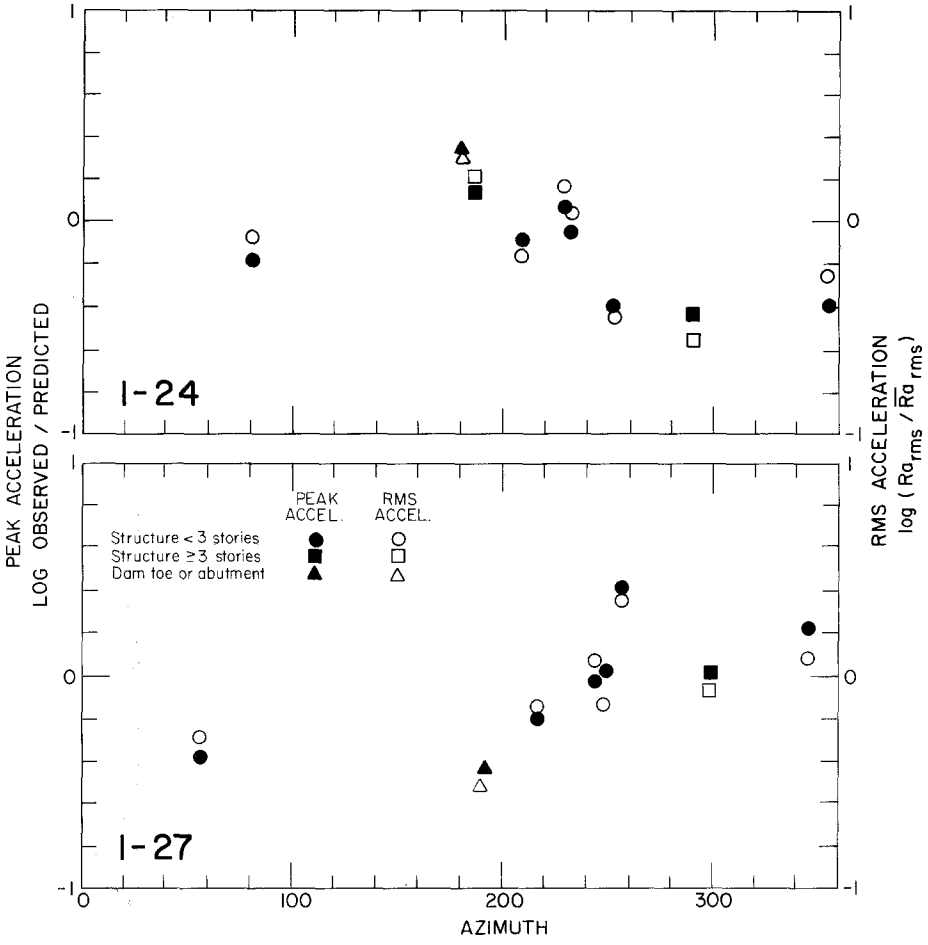

FIG. 10. Comparison of corrected peak ground acceleration and rms acceleration for the 10 stations at which the rms acceleration was measured. The rms accelerations are corrected for hypocentral distance and divided by the mean, $\overline{Ra}_{rms}$. The solid symbols are the corrected peak accelerations; the open symbols are the corrected rms accelerations.

This spectral model is appropriate for the aftershock. Here $\rho = 2.8$ gm/cm^3 and $\beta = 3.3$ km/sec are the density and the shear wave velocity, and we assume $v = 0.75\beta$ is the average rupture velocity, $\Delta v = 0.85\beta$ is the change of rupture velocity associated with the radiated accelerations, and $\bar{\mathcal{R}}^s = 0.77$ is the average *high-frequency* radiation pattern for *SH* waves which takeoff between 10° and 40° from the horizontal from a strike-slip fault (see Boatwright, 1982, Figures 1 and 2), multiplied by two to account for the free-surface. The effect of the near-surface density, $\rho' = 2.5$ gm/cm^3, and shear wave velocity, $\beta' = 1.5$ km/sec, on the acceleration amplitudes is approximated by the factor $(\rho'\beta'/\rho\beta)^{1/2} = 0.64$ (Aki and

Richards, 1980). Using the estimates of R, a_{rms}, and f_{max} listed in Table 2, with $f_0 =$ 0.7 Hz for the main shock and 0.9 Hz for the aftershock, then gives estimates of the rms dynamic stress drop of $\Delta\sigma = 152 \pm 29$ bars for the main shock and 173 ± 26 bars for the aftershock.

The estimate of the dynamic stress drop of the aftershock can be tested against the initial slope technique proposed by Boatwright (1980), where

$$\tau_c = \rho \left(\frac{\beta}{v}\right)^3 \frac{R}{F^s}(1 - \zeta^2)^2 \left\langle \frac{\dot{u}}{t} \right\rangle . \tag{4}$$

In this equation, $\zeta = \frac{v}{\beta} \sin\theta$, where θ is the angle between the takeoff direction of the ray and the normal to the fault surface. The measurements of the initial slope of the velocity waveforms, $\left\langle \frac{\dot{u}}{t} \right\rangle$, are listed in Table 3 along with the resulting estimates of the dynamic stress drop. The radiation pattern correction, $F^s = 1.1$, is the average of the absolute value of the SH radiation pattern over the range of the

TABLE 3

DYNAMIC STRESS DROP DATA

Station	R (km)	θ	$\left\langle \frac{\dot{u}}{t} \right\rangle$ (cm/sec^2)	$\Delta\sigma$ (bars)
A3E	35.1	10°	18.4	246
ANT	32.1	85°	47.4	119
DPP	18.0	35°	31.2	145
MSJ	33.9	35°	13.9	122
SRE	23.5	22°	109.1	855
WCS	36.6	40°	21.7	184
FR	15.6	60°	77.0	155

takeoff angles, multiplied by two to correct for the free surface. The measurements of the initial slope were corrected for attenuation by subtracting $t^*/2$ ($= T/2Q$ where T is the travel time and $Q = 200$) from the duration over which the slope was estimated. The resulting estimate of the dynamic stress drop is 162 ± 18 bars, slightly less than the estimate of the rms dynamic stress drop determined from the rms accelerations.

These estimates of the dynamic stress drop are somewhat larger than the a_{rms} stress drops determined by Hanks and McGuire (1981) for seven moderate aftershocks of the 1975 Oroville, California, earthquake, whose a_{rms} stress drops ranged from 90 to 170 bars. The depths of the aftershocks studied ranged from 6 to 11 km, and they had predominantly normal faulting mechanisms. As the a_{rms} stress drops returned by Hanks and McGuire's (1981) inversion underestimate the rms dynamic stress drops by about 20 per cent (Boatwright, 1982), the estimates of stress drop from these two different tectonic environments appear to be remarkably similar.

THEORETICAL RELATIONS BETWEEN PEAK AND RMS ACCELERATION

The correlation between the peak accelerations and the rms accelerations shown in Figure 10 suggests comparing these measurements to predictions from theoretical

models of the acceleration waveforms. We will consider two models: the deterministic model proposed by Boatwright (1982) and the stochastic model similar to the model of Hanks and McGuire (1981). From equation (6) of Boatwright (1982), the peak acceleration radiated by a subevent of radius r' and dynamic stress drop $\Delta\sigma'$ may be written as,

$$a_{\max} = \frac{\Delta\sigma'}{\mu} \frac{\mathcal{R}^s}{R} \frac{r'}{\zeta} \Delta v \tag{5}$$

where ζ is the width of the acceleration pulse, $\zeta a_{\max}$ is the area under the acceleration pulse, and μ is the rigidity. Dividing the area of the acceleration pulse by the rms acceleration and assuming that the dynamic stress drop of the strongest subevent ($\Delta\sigma'$) is greater than or equal to the rms dynamic stress drop of the overall event ($\Delta\sigma$), equations (3b) and (5) determine an upper bound for the radius of the subevent which radiated the peak acceleration

$$\frac{\zeta a_{\max}}{a_{rms}} = \frac{2}{3} \frac{\Delta\sigma'}{\Delta\sigma} \frac{r'}{v}. \tag{6}$$

This relation has the same dimensions as equation (25) of McGarr (1981) which relates the asperity radius to the ratio of the peak velocity to the peak acceleration. Because it uses the area of the peak acceleration pulse rather than the peak acceleration, however, it is nearly independent of the attenuation. Note that the use of equation (3b) presumes that the acceleration spectra are peaked and falloff as ω^{-1} above the corner frequency.

Figure 11 shows the measurements made on a number of the accelerograms written by the 27 January aftershock. The measurements are listed in Table 4. The peak accelerations were calculated from the rotated *SH* components rather than by using the values listed in Table 1. If the rms accelerations were calculated from the components on which the peak accelerations were originally measured, the results would be identical. The only anomalous pulse area is the pulse area of the main shock accelerogram recorded at SRE. As shown in Figure 7, this accelerogram has an unusually broad pulse which is not seen on the stations which are near the same azimuth from the event. If we omit this station, we obtain $r'/v \leqq 0.56 \pm 0.04$ sec for the main shock and $r'/v \leqq 0.62 \pm 0.04$ sec for the aftershock. The distribution of the ratios of pulse area to a_{rms} is well constrained for both events.

If the dynamic stress drop of the subevent is approximately equal to the rms dynamic stress drop of the whole event, equation (6) can be used to estimate the radius of the subevent. Assuming that the average rupture velocity is 0.75β where the shear wave velocity at depth is 3.3 km/sec, we obtain 1.5 ± 0.1 km for the radius of one aftershock. This estimate of source size is slightly smaller than the spatial extent of the aftershock cluster which followed this event. For the mainshock, equation (6) gives an upper bound of 1.3 ± 0.1 km for the strongest subevent. We cannot identify a specific section of the aftershock distribution which might correspond to this subevent.

Equation (6) is a deterministic analog of the stochastic relation derived by Hanks and McGuire (1981), which relates the peak acceleration to the rms acceleration by assuming that the ground acceleration in a body wave arrival is finite duration and

bandlimited. Their equation is the first term of the relation,

$$\frac{a_{\max}}{a_{rms}} = [2\ln(2N)]^{1/2} + \frac{\gamma}{[2\ln(2N)]^{1/2}}, \tag{7}$$

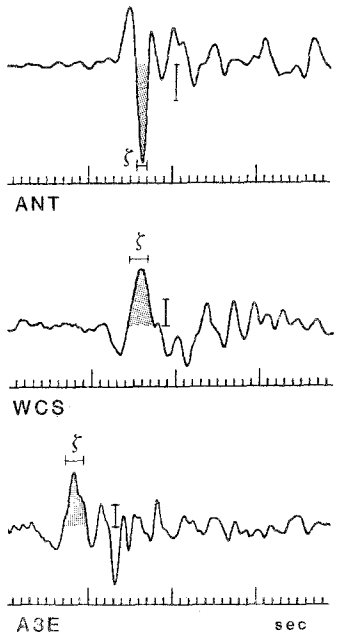

FIG. 11. The measurements of pulse width and peak acceleration for three of the accelerograms written by the 24 January aftershock, shown relative to the rms acceleration level for each pulse.

TABLE 4

PEAK ACCELERATION PULSE DATA

Station	24 January Event			27 January Event		
	$a_{\max}$ (cm/sec^2)	ζ (sec)	$\zeta a_{\max}$ (cm/sec)	$a_{\max}$ (cm/sec^2)	ζ (sec)	$\zeta a_{\max}$ (cm/sec)
A3E	69	0.10	6.9	48	0.17	8.2
ANT	40	0.23	9.2	97	0.13	12.6
DPP	121	0.16	19.4	65	0.17	11.4
DVD	260	0.14	36.4	41	0.21	8.6
MSJ	48	0.14	6.7	44	0.22	9.7
SRE	154	0.28	43.1	235	0.16	37.6
SRM	33	0.13	4.3	56	0.15	8.4
VLR	135	0.19	25.6	54	0.10	5.4
WCS	22	0.12	2.7	45	0.21	9.5
FR	Station Not Installed			178	0.15	26.7

which is itself asymptotic to an exact expression given by Cartwright and Longuet-Higgins (1956). In equation (7), γ is Euler's constant (0.5772...), and N is the average number of positive zero crossings in the duration of strong ground shaking, τ. N may be estimated from zeroth and second moments of the energy spectrum (a more complete analysis of the seismological applications of the results from random

vibration theory is in preparation). Using $\tau = 1.5$ and 1.1 sec for the main shock and the aftershock, respectively, and estimating N from a spectral shape which approximates the data spectra, gives $a_{max} = 2.5a_{rms}$ for the main shock and $a_{max} = 2.4a_{rms}$ for the aftershock. Averaging the ratios of the peak and rms accelerations measured from the accelerograms for each event gives $a_{max} = (2.5 \pm 0.1)a_{rms}$ for both events. Considering the strong directivity in these accelerations, the agreement between the statistical theory and the observations is remarkable.

Peak Velocity and Radiated Energy Flux

It is important to consider how the measurements of peak velocity and radiated energy flux vary with azimuth, and whether they are as strongly correlated as the peak and rms acceleration. The peak velocities, measured from the integrals of the *SH* accelerograms analyzed in the last two sections, are listed in Table 4. They were corrected for epicentral distance using the relation,

$$\log v_{max} = -0.67 + 0.489M - \log r - 0.00256r + 0.17S \qquad (8)$$
$$r = (d^2 + 4.0^2)^{1/2}$$

of Joyner and Boore (1981). In this relation, S takes a value of 1 for soil sites and 0 for rock sites. Stations ANT, MSJ, SRE, and SRM were assumed to be soil sites; the other free-field and large structure stations were assumed to be rock sites. The corrected peak velocities are plotted as a function of azimuth in Figure 12. While not identical to the variation of the corrected peak and rms accelerations shown in Figure 10, the variation with azimuth is similar. Excluding the stations SRM and SRE, which are severely contaminated by their strong site responses, the total variation is estimated to be a factor of 5 (0.7 log units) for both events.

The radiated energy flux in the S waves is calculated by integrating the square of the ground velocity over time or frequency, after correcting for the attenuation. This correction is determined using Parseval's relation,

$$\varepsilon = \frac{\rho\beta}{\pi}\int_0^\infty \dot{u}^2(\omega)e^{\omega t^*}\,d\omega = \rho\beta I^*, \qquad (9)$$

where ρ and β are the density and the shear wave velocity at the receiver, and I^* is the integral of the square of the ground velocity after correcting for attenuation. The necessary measurements are compiled in Table 4. Both the uncorrected and corrected integrals of the square of the ground velocity (I and I^*) are listed to show how the attenuation correction affects the estimate of the radiated energy flux. The station estimates of the total radiated energy are shown in the last column; these estimates are obtained from the relation,

$$E_s = 2\pi\left(\frac{R}{_{FS}}\right)^2 \varepsilon, \qquad (10)$$

(Randall, 1973; Boatwright, 1980). Here the radiation pattern, $_{FS} = 1.25$, is the rms *SH* radiation pattern averaged over the range of takeoff angles and multiplied by two to account for the free surface. The estimates of the radiated energy, compiled in Table 5, vary over a factor of 30 for the main shock and 15 for the aftershock. Because this estimate is determined from a squared measure of the ground motion,

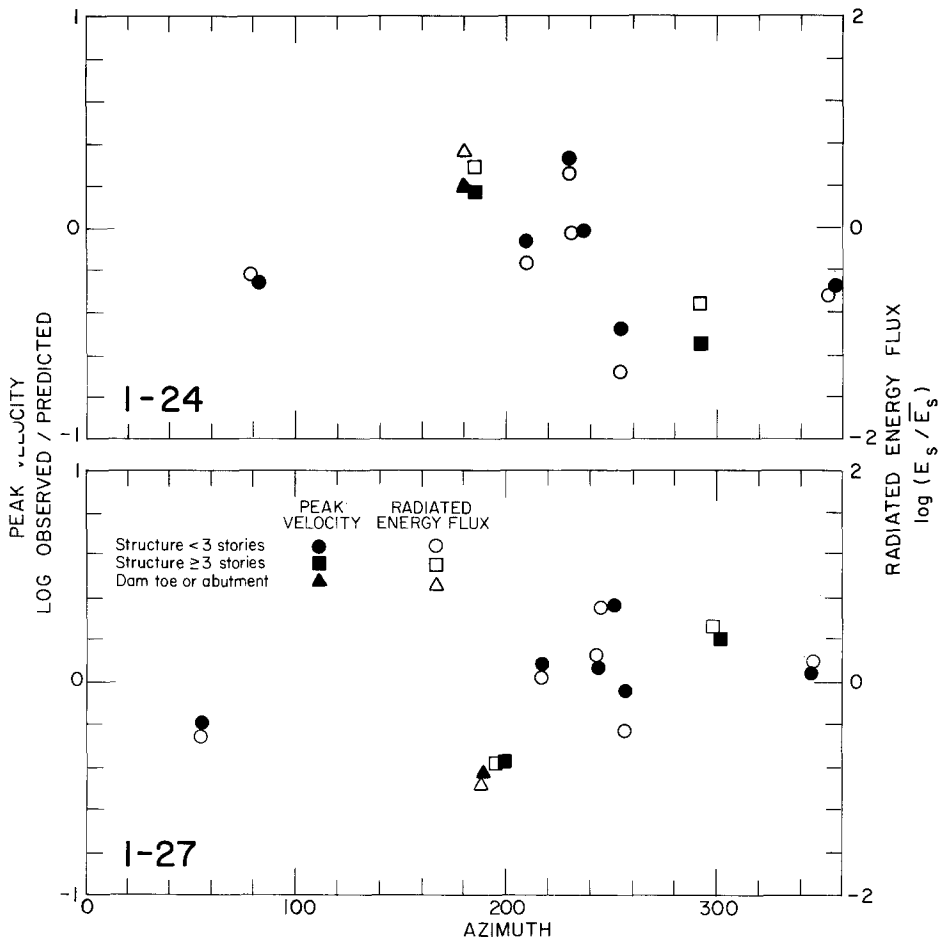

FIG. 12. Corrected peak velocity and radiated energy estimates plotted against azimuth for 10 stations. The stations SRE (at 229° and 256°) and SRM (at 253° and 274°) have anomalous site responses. The open symbols are the corrected radiated energy estimates; the solid symbols are the corrected peak velocities. Note the strong correlation for the 27 January data.

TABLE 5

PEAK VELOCITY AND ENERGY FLUX DATA

Station	24 January Event				27 January Event			
	v_{max} (cm/sec)	I (cm²/sec)	I^* (cm²/sec)	E_s (10^{20} dyne-cm)	v_{max} (cm/sec)	I (cm²/sec)	I^* (cm²/sec)	E_s (10^{20} dyne-cm)
A3E	3.9	8.2	17.7	2.6	3.7	6.6	11.3	1.9
ANT	4.5	7.0	9.6	0.7	6.0	6.4	12.4	1.8
DPP	7.1	22.5	31.3	1.0	5.5	13.3	16.6	0.8
DVD	15.8	81.9	111.2	7.0	2.1	2.2	3.4	0.2
MSJ	3.9	5.6	13.0	2.1	4.5	8.1	12.9	4.5
SRE	21.1	214.4	253.3	13.6	17.5	82.2	115.4	8.9
SRM	2.3	3.4	5.7	0.4	3.7	9.2	14.6	1.5
VLR	14.1	92.5	115.4	6.8	2.6	2.7	4.8	0.3
WCS	2.3	1.1	1.9	0.2	4.9	12.2	19.1	3.6
FR	Station Not Installed				12.4	30.5	41.2	1.4

the square roots of these factors (5.5 and 4) should be compared to the variation of the peak velocity.

Such a strong variation can lead to substantial errors in estimates of the radiated energy for unilateral ruptures. The average radiated seismic energies are estimated as $2.6 \pm 0.9 \times 10^{20}$ dyne-cm for the main shock and $1.5 \pm 0.3 \times 10^{20}$ dyne-cm for the aftershock by calculating the arithmetic average of the station estimates. As the ratio of the moments of the events calculated by Bolt *et al.* (1981) was about 3, the aftershock appears to have radiated energy more efficiently than the main shock. This discrepancy may result in part from the station distribution; the aftershock ruptured toward the largest concentration of stations (to the northwest) whereas the main shock ruptured away from these stations.

The correlation between the peak velocities and radiated energies shown in Figure 12 is as strong as the correlation between the peak and rms accelerations, particularly for the 27 January aftershock recordings. SRM is the only anomalous station: the corrected radiated energy is approximately 50 per cent less than the corrected peak velocity. The azimuthal variation of these measurements appears to be about two-thirds the variation of the peak accelerations. Comparison of Figure 12 to Figure 10 indicates that the velocity measurements do not correlate with the acceleration measurements as well as they correlate with each other.

The stochastic relation of the peak velocity to the rms velocity is similar to the relation between the peak and rms acceleration. They differ only in the number of positive zero crossings. N is smaller for velocity pulse shapes than for acceleration pulse shapes because velocity spectra have a lower dominant frequency than acceleration spectra. For the velocity spectra from these two events, N is small enough to require using the exact expression to which equation (7) is asymptotic. This expression predicts that the ratio of peak velocity to the rms velocity is bounded as $2.3 \geqq v_{\max}/v_{rms} \geqq 1.7$, for velocity spectra which falloff between ω^{-1} and ω^{-2} above the corner frequency. Using the values of $v_{\max}$ and I listed in Table 5 and the relation,

$$v_{rms} = \left(\frac{I}{\tau}\right)^{1/2}, \tag{11}$$

to determine averages of the ratios of the peak velocity to the rms velocity, gives $v_{\max} = (1.9 \pm 0.1)v_{rms}$ for the main shock and $v_{\max} = (1.7 \pm 0.1)v_{rms}$ for the aftershock. As noted previously, the velocity spectra from the main shock rolloff as ω^{-1} over a narrow frequency band while the spectra from the aftershock rolloff as ω^{-2} above the corner frequency. The observations are in excellent agreement with the theoretical predictions.

Discussion

Directivity in these earthquakes was also observed in longer period motions, including Wood-Anderson seismographs and broadband recorders (Bolt *et al.*, 1981; Schechter, 1981). Figure 13, adapted from Schechter (1981), compares the Wood-Anderson seismograms recorded at Arcata and Santa Barbara. The azimuth from the main shock to Santa Barbara is within 10° of the assumed direction of rupture; the difference in amplitude between SBC and ARC is about a factor of 10. For the aftershock, however, the difference is less pronounced. The low-magnification, Wood-Anderson equivalent at Berkeley gave magnitudes of 5.5 and 5.9 for the first and second events, respectively. If the magnitudes had been based on peak accelerations, the theoretical curve in Figure 9 predicts that the difference between first and second events would have been 0.5 to 0.7 units, depending on the change of

rupture velocity. The observed difference of 0.4 corresponds to the expected difference in peak velocity rather than peak acceleration. The relative amplitudes of the broadband recordings at Berkeley are reversed with respect to the Wood-Anderson amplitudes, with the first event having much more long-period motion (B. Schechter, written communication, 1981). This behavior reflects the relative size of the moments of the two events.

The strong directivity in the peak accelerations radiated by these earthquakes implies that both events had unilateral ruptures. In equation (5), the peak acceleration depends linearly on the asperity radius and the dynamic stress drop. For an incoherent rupture in which the dynamic stress drop is approximately constant over the component subevents, the directivity in the radiated peak accelerations must be similarly reflected in the relative asymmetry of the rupture process. Either the peak accelerations were radiated by an extremely large and unilateral subevent, or all the larger subevents ruptured in the same direction. A similar argument can be made

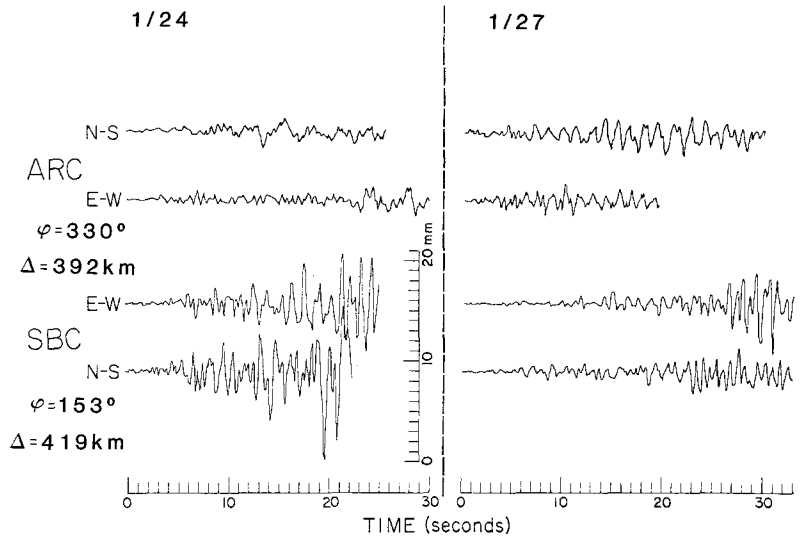

FIG. 13. Wood-Anderson seismograms of the 24 January main shock and the 27 January aftershock recorded at Arcata and Santa Barbara (reprinted from Schechter, 1981).

concerning the directivity in the rms acceleration measurements. Because the rms acceleration is the mean of the *square* of the acceleration, it is most sensitive to the strongest subevent. For complex events, then, both the peak and rms acceleration should be generally insensitive to directivity, except in the case of a simple event or a purely unilateral rupture. The fact that the peak and rms accelerations show such strong directivity implies that the rupture processes of these earthquakes were unilateral.

In the analysis of these accelerations, we have emphasized the difference between the average rupture velocity, v, and the change in rupture velocity, Δv, which controls the high-frequency radiation. The average rupture velocity is strongly conditioned by the complexity and geometry of the rupture growth. For simple ruptures, it may approach the terminal rupture velocities for antiplane and inplane cracks, i.e., the shear and Rayleigh wave speeds. For complex ruptures, however, it will be substantially slower. In contrast, the radiative change in rupture velocity is a property of the crack tip, or the set of crack tips making up a complex rupture

process. It should be close to the terminal rupture velocity, regardless of the complexity of the rupture process. The lower bound of $\Delta v = 0.7\beta$ determined from the directivity in the radiated peak accelerations is substantially slower than these terminal velocities. The range of takeoff angles and the possibility of a subhorizontal rupture direction may have weakened the observed directivity, however. This lower bound is commensurate with the estimate of $\Delta v = 0.80 \pm 0.07\beta$, obtained by Boatwright (1982) from a comparison of the high-frequency content of the P and S waves radiated by 10 small earthquakes in Monticello, South Carolina.

Conclusions

The peak horizontal accelerations, the rms accelerations, the peak velocities, and the energy flux radiated by the main shock and the largest aftershock of the 1980 Livermore Valley earthquake sequence show clear evidence of directivity, both for each event individually and in the ratio of the motions at common recording sites. The azimuthal variation of the accelerations, corrected for the geometrical spreading and attenuation, was as much as a factor of 10. A theoretical model for the directivity in the accelerations fits the data well. While the radiative change of rupture velocity cannot be determined uniquely from the data, it appears to support the lower bound of $\Delta v = 0.7\beta$.

Although we have established the significant impact that directivity had on the S waves in accelerograms from the 1980 Livermore Valley earthquakes, we make no claim for being the first to establish conclusively directivity at high frequencies. For example, Bakun *et al.* (1978) showed clear directivity effects in a study of P waves from two small magnitude earthquakes (M = 3.0 and 2.0) in central California. However, this analysis is the first to clearly demonstrate directivity in the high-frequency accelerations which are of interest to seismic engineers. Moreover, the measurements analyzed in this study, i.e., peak acceleration, rms acceleration, peak velocity, and radiated energy flux, are of more importance to seismic engineering than the duration and frequency of zero crossing measurements analyzed by Bakun *et al.* (1978).

The correlations between the peak and rms accelerations, and the peak velocities and the radiated energy flux imply that the measurements of peak acceleration and peak velocity made on a large number of accelerograms and seismograms can be used to determine source parameters such as the dynamic stress drop and the radiated seismic energy if the signal durations are also measured. In particular, the relations between peak velocity, rms velocity, signal duration, and radiated energy flux might be used to supplant the Gutenberg-Richter magnitude-energy relationship (Richter, 1958), if broadband instruments are used.

While it is possible that a future earthquake could exhibit a more extreme directivity in its radiated wave field, it is suggested that this data set be used as an upper bound for the expected effect of directivity. For peak and rms acceleration, the maximum total variation is a factor of 10, or a factor of 3 amplification of the mean. For peak velocity, the total variation is a factor of 5, while the energy flux can vary by a factor of 30. Finally, the total variation expected from differential site effects, including soil response and structural resonances, appears to be a factor of 3.

Acknowledgments

We thank Rob Cockerham for the aftershock locations which are shown in Figures 2 and 3, Ron Porcella for the peak acceleration measurements, and Bruce Schechter for use of the Wood-Anderson recordings shown in Figure 13. This paper has been critically reviewed by Art McGarr, Jim Scheimer, and Paul Spudich, whose comments have helped us to improve it significantly.

REFERENCES

Aki, K. and P. G. Richards (1980). *Quantitative Seismology: Theory and Methods*, W. H. Freeman, San Francisco.

Archuleta, R. J. (1979). Rupture propagation effects in the Coyote Lake earthquake (abstract), *EOS, Trans. Am. Geophys. Union* **60**, 890.

Bakun, W. H., R. M. Stewart, and C. G. Bufe (1978). Directivity in the high-frequency radiation of small earthquakes, *Bull. Seism. Soc. Am.* **68**, 1253–1263.

Benioff, H. (1955). Mechanism and strain characteristics of the White Wolf fault as indicated by the aftershock sequence, *Earthquakes in Kern County, California during 1955* (G. B. Oakeshott, Editor), *Calif. Div. Mines Bull.* **171**, 199–202.

Boatwright, J. (1980). A spectral theory for circular seismic sources: simple estimates of source dimension, dynamic stress drop and radiated seismic energy, *Bull. Seism. Soc. Am.* **70**, 1–27.

Boatwright, J. (1982). A dynamic model for far-field acceleration, *Bull. Seism. Soc. Am.* **72**, 1049–1069.

Bolt, B. A., T. V. McEvilly, and R. A. Uhrhammer (1981). The Livermore Valley, California, sequence of January 1980, *Bull. Seism. Soc. Am.* **71**, 451–463.

Boore, D. M. and R. L. Porcella (1980). Peak acceleration from strong-motion records: a postscript, *Bull. Seism. Soc. Am.* **70**, 2295–2297.

Boore, D. M., W. B. Joyner, A. A. Oliver, III, and R. A. Page (1980). Peak acceleration, velocity, and displacement from strong-motion records, *Bull. Seism. Soc. Am.* **70**, 305–321.

Cartwright, D. E. and M. S. Longuet-Higgins (1956). The statistical distribution of the maxima of a random function, *Proc. Roy. Soc. Lond., Ser. A* **237**, 212–232.

Cockerham, R. S., F. W. Lester, and W. L. Ellsworth (1980). A preliminary report on the Livermore Valley earthquake sequence January 24–February 26, 1980, *U.S. Geol. Surv., Open-File Rept. 80-714.*

Hanks, T. C. and R. K. McGuire (1981). The character of high-frequency strong ground motion, *Bull. Seism. Soc. Am.* **71**, 2071–2096.

Joyner, W. B. and D. M. Boore (1981). Peak horizontal acceleration and velocity from strong-motion records including records from the 1979 Imperial Valley, California, earthquake, *Bull. Seism. Soc. Am.* **71**, 2011–2038.

Madariaga, R. (1977). High-frequency radiation from crack (stress-drop) models of faulting, *Geophs. J.* **51**, 625–652.

McCann, M. and D. M. Boore (1982). Variability in ground motions: root mean square accelerations and peak acceleration for the 1971 San Fernando, California, earthquake, *Bull. Seism. Soc. Am.* (in press).

McGarr, A. (1981). Analysis of peak ground motion in terms of a model of inhomogeneous faulting, *J. Geophys. Res.* **86**, 3901–3912.

McGuire, R. K. and T. C. Hanks (1980). rms accelerations and spectral amplitudes of strong ground motion during the San Fernando, California, earthquake, *Bull. Seism. Soc. Am.* **70**, 1907–1919.

McJunkin, R. D. and J. T. Ragsdale (1980). Strong-motion records from the Livermore earthquake of 24 and 26 January 1980, *Calif. Div. Mines and Geology Preliminary Report 28.*

Randall, M. J. (1973). The spectral theory of seismic sources, *Bull. Seism. Soc. Am.* **63**, 1133–1144.

Richter, C. A. (1958). *Elementary Seismology*, W. H. Freeman, San Francisco, 768 pp.

Savage, J. C. (1965). The stopping phase on seismograms, *Bull. Seism. Soc. Am.* **58**, 47–58.

Schechter, B. (1981). Source parameters and directivity of the Livermore earthquakes of 1980 (abstract), *Earthquake Notes* **52**, 83.

Swanger, H. J., S. M. Day, J. R. Murphy, and R. Guzman (1981). State-of-the-Art study concerning near-field earthquake ground motion, U.S. Nuclear Reg. Comm. NUREG/CR-1978.

Switzer, J., D. Johnson, R. Maley, and R. Matthiesen (1981). Western hemisphere strong-motion accelerograph station list-1980, *U.S. Geol. Surv., Open-File Rept. 81-664.*

U.S. GEOLOGICAL SURVEY
OFFICE OF EARTHQUAKE STUDIES
345 MIDDLEFIELD ROAD
MENLO PARK, CALIFORNIA 94025

Manuscript received 19 March 1982